SCIENTIFIC REPORTS

OPEN

Improvement of infrared single-photon detectors absorptance by integrated plasmonic structures

Mária Csete[1,2], Áron Sipos[2], Anikó Szalai[2], Faraz Najafi[1], Gábor Szabó[2] & Karl K. Berggren[1]

[1]Massachusetts Institute of Technology, Research Laboratory of Electronics, 77 Massachusetts Avenue, Cambridge, Massachusetts, USA 02139, [2]University of Szeged, Department of Optics and Quantum Electronics, H-6720, Szeged, Dóm tér 9, Hungary.

Plasmonic structures open novel avenues in photodetector development. Optimized illumination configurations are reported to improve p-polarized light absorptance in superconducting-nanowire single-photon detectors (SNSPDs) comprising short- and long-periodic niobium-nitride (NbN) stripe-patterns. In OC-SNSPDs consisting of ~quarter-wavelength dielectric layer closed by a gold reflector the highest absorptance is attainable at perpendicular incidence onto NbN patterns in P-orientation due to E-field concentration at the bottom of nano-cavities. In NCAI-SNSPDs integrated with nano-cavity-arrays consisting of vertical and horizontal gold segments off-axis illumination in S-orientation results in polar-angle-independent perfect absorptance via collective resonances in short-periodic design, while in long-periodic NCAI-SNSPDs grating-coupled surface waves promote EM-field transportation to the NbN stripes and result in local absorptance maxima. In NCDAI-SNSPDs integrated with nano-cavity-deflector-array consisting of longer vertical gold segments large absorptance maxima appear in 3p-periodic designs due to E-field enhancement via grating-coupled surface waves synchronized with the NbN stripes in S-orientation, which enable to compensate fill-factor-related retrogression.

The near-field enhancement accompanying the localized and propagating surface plasmon polaritons' (SPP) excitation is an extensively studied phenomenon in nanophotonics[1–6]. Single metal-dielectric composite objects confine and transport the EM-field via localized plasmonic modes, e.g. via hybrid waveguide modes in slits[7–10] and via strongly squeezed plasmonic modes in open[11] and closed sub-wavelength MIM nano-cavities[12]. Arrays of slits exhibit resonant transmission phenomena[13–20], while arrays of closed cavities, namely the nano-cavity gratings[21–25], are capable of resulting in resonant absorption. These complex plasmonic structures are the most promising in different application areas, since the highest degree of freedom is attainable in spectral bands' engineering by controlling the interaction of all supported localized plasmonic and propagating surface modes via predesigned geometry[13–25]. The sensitivity of the coupling efficiency to the relative E-field oscillation direction with respect to plasmonic structures[26] makes possible to control the near-field confinement around single nano-objects[7–12] and to attain collective resonance phenomena[13–25] via periodic patterns with optimized geometry.

The spectral and near-field effects of plasmonic structures are widely applied in different areas of nano-photonics including improvement of high harmonic generation[25], directional out-coupling from LEDs[27,28], enhancement of emission[29–31], control of laser beam-shape[32], optimization of bio-sensors' sensitivity[33] and photo-detectors' efficiency[10,16,34–40]. Plasmonic structures with different geometry, namely sub-wavelength metal nano-islands[34], nano-antennas[35,40], dielectric loaded slot waveguides[10], linear slit-arrays[16], as well as gratings with linear, circular and hexagonal symmetry[36–40] were integrated into versatile photodetectors.

An emerging plasmonic structure application area is the improvement of superconducting nanowire single-photon detectors' (SNSPDs) efficiency[41]. Conventional SNSPD devices consist of a meandered niobium-nitride (NbN) stripe pattern as an absorbing element.

Detection efficiency larger than 90% was attained recently via non-plasmonic approaches as well, by applying dielectric waveguide-coupled NbN wires[42], and via novel superconducting material and substrate combination, namely by aligning WSi wires onto silicon-based optical stack[43]. However, NbN wires appropriately long to result in enhanced absorptance cause simultaneously increased decay time in waveguide-coupled SNSPDs[42], as a consequence do not meet the reset-time requirements. The fiber-coupled WSi wire consisting devices approach the ideal performance, however specific applications require full polarization control[43].
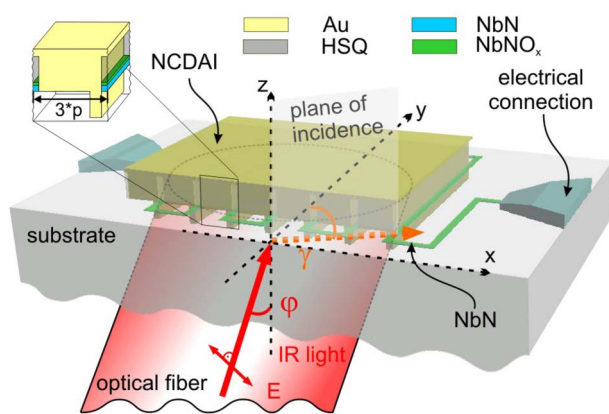
Figure 1 | Illumination of nano-cavity-deflector-array integrated NCDAI-SNSPD device designs in conical mounting.

Novel approaches based on plasmonic structures' integration into SNSPDs open novel avenues in secure communication and in quantum-key computing as well[44–50]. The most simple noble metal structure integrated into SNSPDs was a thin gold reflector aligned onto the top of quarter-wavelength dielectric cavity, which made possible to reach ~50% absorptance[45–47]. Our previous studies have proven that it is possible to squeeze the EM-field around the nanometric NbN stripes via resonant nano-plasmonic modes supported by nano-cavities[48–50]. The E-field expelling from noble metal segments and the coupling to localized plasmonic modes enable to exceed ~90% absorptance in short-periodic (200 nm), and ~40% absorptance in long-periodic (600 nm) nano-cavity-array integrated

SNSPD designs at perpendicular incidence[49,50]. Moreover, our previous results have shown that integration of appropriately designed complex nano-cavity-arrays' results in IR light concentration around the tiny NbN segments via grating-coupled surface modes at specific orientations[50].

Besides device geometry development of SNSPDs, the effect of illumination direction was investigated as well, and the possibility of absorptance improvement via total internal reflection (TIR)[47,51], resonant plasmonic[48–50], and equivalent Brewster angle related[50] phenomena was demonstrated. It was shown that in periodic plasmonic structure integrated SNSPDs those orientations are the most advantageous, where the E-field oscillation direction is perpendicular to the noble metal segments[48–50].

The methodology applied to investigate the effect of illumination direction during p-polarized light illumination of complex plasmonic structure integrated SNSPD devices is presented in Fig. 1. In present theoretical study the optimal illumination directions were determined via numerical method for three different SNSPD device designs consisting of (1) ~quarter-photonic-wavelength nano-cavity closed by a gold reflector (OC-SNSPD, Fig. 2a, d), (2) nano-cavity-array closed by vertical and horizontal gold segments (NCAI-SNSPD, Fig. 2b, e), and (3) nano-cavity-deflector-array consisting of longer vertical gold segments (NCDAI-SNSPD, Fig. 1 and Fig. 2c, f). Two periodicity intervals were investigated, namely the $p \sim 200$ nm approximating the periodicity of wire-patterns in conventional SNSPD devices, where the detection efficiency is optimized via effective NbN absorptance cross-section maximization[45–50]; and the larger $3p \sim 600$ nm periodicity, capable of ensuring simultaneous electrical optimization due to the reduced kinetic inductance of shorter wires, similarly to references[49,50].
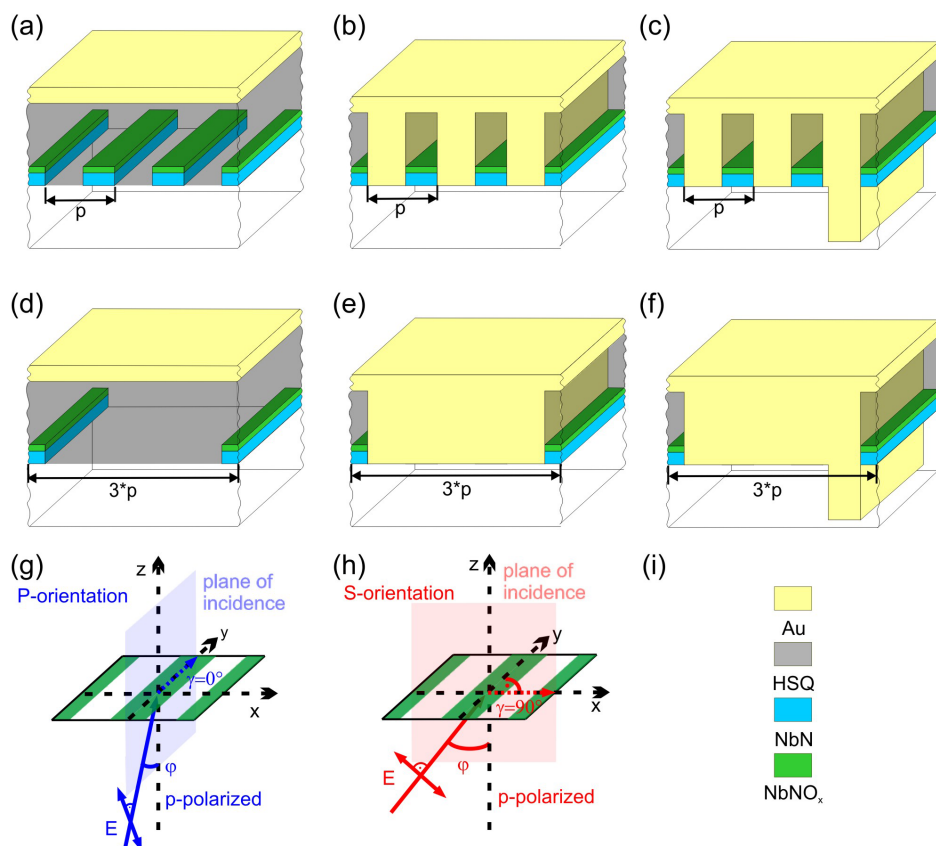

Figure 2 | Schematic drawings of device designs with periodicities $p = 200$ nm, 220 nm and 237 nm/$3p = 600$ nm, 660 nm and 710 nm. (a)/(d) OC-SNSPD, (b)/(e) NCAI-SNSPD, (c)/(f) NCDAI-SNSPD. The configurations applied to realize p-polarized illumination (g) in P-orientation, and (h) in S-orientation. The (i) insets indicate the identification of materials in the integrated SNSPD devices.

The purpose of our present work was to determine the geometrical parameters of plasmonic structures most appropriate to enhance absorption in p- and 3p-periodic meandered NbN patterns via unique nanophotonical phenomena, and to determine the optimal illumination directions for integrated SNSPD device designs. The concept of E-field concentration via localized plasmonic modes and via surface waves coupled by the periodic integrated structures was applied to enhance the effective extinction cross-section of the NbN pattern.

Finite element method was applied to determine the optical response and near-field distribution following the numerical approach described in our previous paper[46]. The optimal directions were determined for 1550 nm wavelength p-polarized light illumination by three-dimensional computations allowing arbitrary polar and azimuthal orientations (specified by φ and γ in Fig. 1 and 2g, h) of the integrated devices. Spectral studies were performed at those orientations of specific SNSPD designs, which correspond to NbN absorptance maxima on the angle dependent optical responses.

To analyze the illumination direction dependence of the integrated systems' spectral response in details, the wavelength and angle of incidence were simultaneously varied in the intervals corresponding to significant NbN absorptance modifications in NCAI- and NCDAI-SNSPDs. The wavelength dependent NbN absorptance of one specific design was computed at each representative extrema in polar angle (see Supplementary material).

The geometry of individual NbN stripes is in accordance with those in conventional SNSPDs, but three different NbN pattern periodicities (200 nm, 220 nm, 237 nm and 600 nm, 660 nm, 710 nm) were inspected in both short p- and long 3p-periodicity regions for OC-, NCAI- and NCDAI-SNSPD design types.

In OC-SNSPD devices the superconducting NbN pattern is embedded into ~quarter-photonic-wavelength nano-cavity filled with dielectric and closed by a gold reflector (Fig. 2a, d). This OC-SNSPD structure is similar to the device designs described in[45–47], but in our present work three different periodicities are investigated in both p- and 3p-periodicity regions.

In NCAI-SNSPD devices the NbN stripes are aligned at the bottom of ~quarter-plasmon-wavelength nano-cavities, which are closed by vertical and horizontal gold segments, and compose plasmonic MIM nano-cavity-array with p- and 3p-periodicity (Fig. 2b, e).

The entirely novel NCDAI-SNSPD device design is based on nano-cavity-deflector-array consisting of longer vertical gold segments. In order to minimize the spurious gold absorptance, as well as to maintain the commensurability of the periodicity with the wavelength of the supported surface waves, same deflector segments with 3p-periodicity were integrated into both p- and 3p-periodic NbN patterns (Fig. 2c, f).

Results

The inspection of the dual-angle-dependent absorptance revealed that each device design has an optimal illumination direction specified by geometry dependent azimuthal (γ) and polar (φ) angles (Fig. 3, 4a, 5, 6a, Supplementary Fig. S1a).

P-polarized illumination of NbN patterns in P-orientation ($\gamma = 0°$) is more efficient in all OC-SNSPDs, while higher absorptance is attainable in S-orientation ($\gamma = 90°$) in all NCAI-SNSPD and NCDAI-SNSPDs, as presented in insets of Fig. 3 and 5. The absorptances in device orientations that are promising for practical applications were compared for three different p- and 3p-periodicities of each design types (Fig. 3, 4a and 5, 6a).

The inspection of the spectral responses of NCAI- and NCDAI-SNSPD designs at the NbN absorptance maxima in polar angle indicated the particularity of one specific 3p-periodicity (Fig. 4b–d and 6b–d, Supplementary Fig. S1b). The investigation of the normalized E-field distribution at the global extrema uncovered the role of localized plasmonic and versatile grating-coupled surface modes in NbN absorptance enhancement (Fig. 7 and 8, Supplementary Fig. S2).

NbN absorptance in short-periodic designs. In all three short-periodic OC-SNSPDs the maximal absorptances (66.4%, 62.7%, 59.9%) are observable at perpendicular incidence (Fig. 3a). Local absorptance perturbations appear at the orientations corresponding to the condition of TIR and surface plasmon polariton excitation phenomena. At larger tilting local maxima are reached at the same ~75° polar angle, which originate from NbN-related ATIR phenomenon. All global and local maxima decrease monotonously by increasing the periodicity in p-periodic OC-SNSPDs.

In short-periodic NCAI-SNSPDs almost tilting independent perfect absorptance is observable through large polar angles (Fig. 3b). The TIR and SPP excitation phenomena manifest themselves in local absorptance perturbations also in these designs at 34.5° and 35.1° polar angles. The 93.8% global absorptance maximum appears at 40° polar angle in 200-nm-pitch design, i.e. approximating the orientation corresponding to SPP excitation, while it is shifted to larger 45° (93.4%) and 50° (93.1%) polar angles in the 220-nm and 237-nm-pitch designs. The global maxima decrease monotonously by increasing the periodicity also in p-periodic NCAI-SNSPDs.

In short-periodic NCDAI-SNSPDs the maximal absorptance (93.5%, 93.3%, 92.4%) is reached at perpendicular incidence, and the NbN absorptance monotonously decreases with the tilting (Fig. 3c). Sudden absorptance modifications are observable, and the corresponding inflection points shift to smaller polar angles by increasing the periodicity. The cut-off and recovery points at sudden slope modifications correspond to global maxima and local minima on the polar angle dependent NbN absorptance of long-periodic
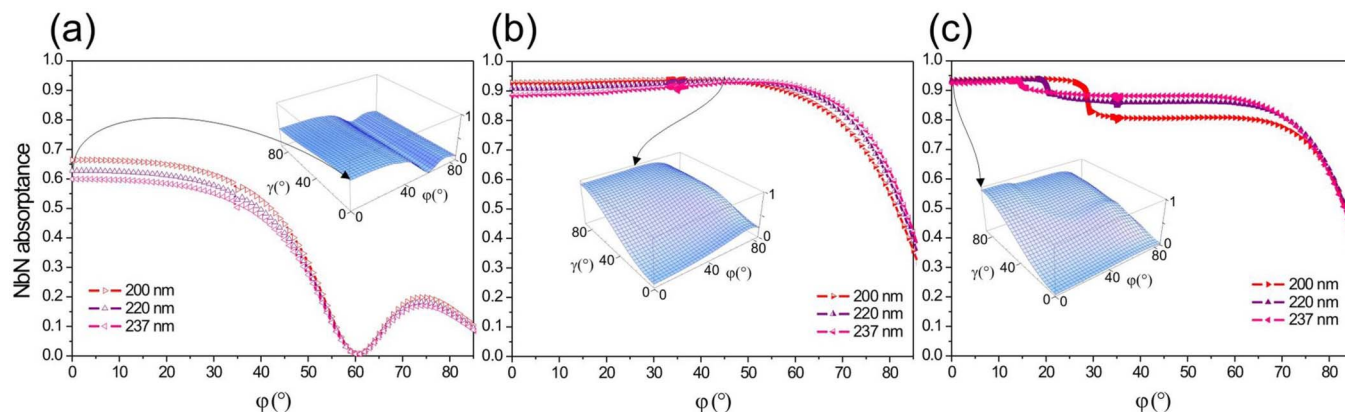

Figure 3 | NbN absorptance in three different short p-periodic SNSPD designs. (a) OC-SNSPD in P-orientation, (b) NCAI-SNSPD in S-orientation, and (c) NCDAI-SNSPD in S-orientation. The insets indicate the polar-azimuthal angle dependent NbN absorptance in 220-nm-pitch designs.
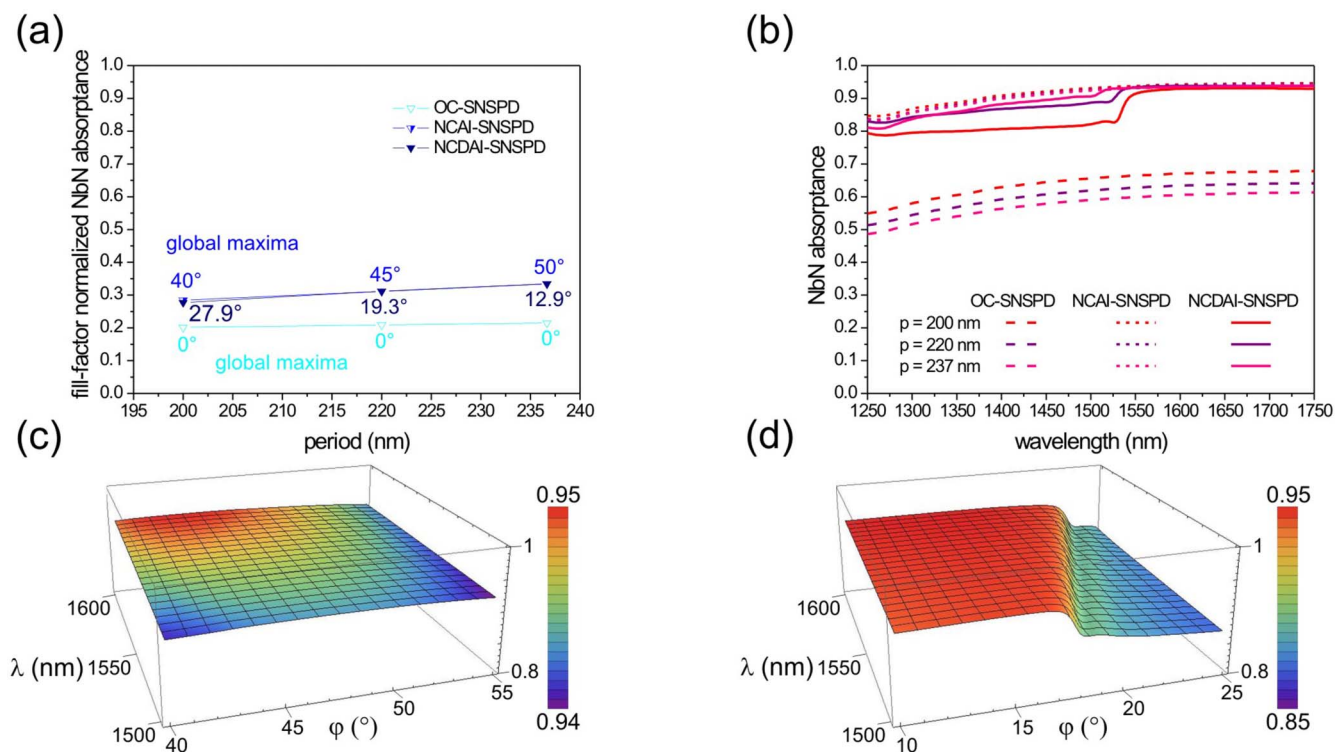
Figure 4 | (a) The NbN absorptance normalized by the fill-factor in *p*-periodic SNSPD designs. (b) Wavelength dependent absorptance at the orientations in different SNSPD designs indicated in (a). The NbN absorptance as a function of φ polar angle and λ wavelength in 220-nm-pitch (c) NCAI-SNSPD and (d) NCDAI-SNSPD design.

NCDAI-SNSPD counterpart-designs (see next section). Additionally, local NbN absorptance maximum is observable in 220 and 237-nm-pitch designs before cut-off, while local minimum appears before recovery in 200-nm-pitch NCDAI-SNSPD. The NbN absorptance attainable at small tilting decreases monotonously by increasing the periodicity in *p*-periodic NCDAI-SNSPDs.

The NbN absorptance was normalized by the ratio of the fill-factor in 660 nm design to the fill-factor in specific designs (Fig. 4a). The normalized absorptance monotonously increases in short-periodic devices by increasing the periodicity, with the smallest values and slope in OC-SNSPDs, indicating that these devices are the less promising in absorptance maximization procedures. Commensurate NbN absorptances are reached in NCAI-SNSPDs and NCDAI-SNSPDs with the same periodicities, but the slope of the normalized absorptance curve is slightly larger in presence of deflectors indicating that larger periodic patterns are more promising in contempt of the gold-to-NbN ratio increase. No particular pitch is identifiable in the interval of *p*-periodicities, according to the sub-wavelength size-scale.

Figure 4b presents that the NbN absorptance monotonously increases with the wavelength at the global maxima in polar angle in *p*-periodic OC- and NCAI-SNSPD designs. Monotonous increase is observable as well as in NCDAI-SNSPDs at those orientations, which correspond to global maxima of counterpart 3*p*-designs, except the 200-nm-pitch design exhibiting a small local minimum. The wavelength dependent NbN absorptance in *p*-periodic NCDAI-SNSPDs indicates sudden slope modifications, and the corresponding inflection points shift to smaller wavelengths by increasing the NbN pattern periodicity. The recovery point appears in the closest proximity of 1550 nm in 220-nm-pitch design.

The orientation dependence of the 220-nm-pitch designs spectra indicate that the NbN absorptance monotonously increases in NCAI-SNSPDs by increasing either the polar angle or the wavelength (Fig. 4c), while the sudden slope modifications occur at larger polar angle in NCDAI-SNSPDs by increasing the wavelength (Fig. 4d).

NbN absorptance in long-periodic designs. In all three long-periodic OC-SNSPDs the maximal absorptance (29.2%, 26.8%, 25.1%) is reached at perpendicular incidence (Fig. 5a, Supplementary Fig. S1a). Local perturbations originating from TIR and SPP excitation phenomena appear at the same tilting, as observed in short-periodic designs. The NbN-related ATIR results in appearance of small local NbN absorptance maxima at ~74° polar angle, analogously with short-periodic OC-SNSPDs. Three-times reduced fill-factor causes considerably smaller global NbN absorptance maxima, than in short-periodic OC-SNSPDs, which decrease monotonously by increasing the periodicity.

In long-periodic NCAI-SNSPDs the absorptance is moderately enhanced (41.2%, 32.3%, 26.6%) at perpendicular incidence in comparison to the OC-SNSPDs with same pitch (Fig. 5b-to-a, Supplementary Fig. S1a). Tilting causes sudden changes in the NbN absorptance, which manifests itself in a global minimum followed by a local maximum and an adjacent local minimum in each 3*p*-periodic NCAI-SNSPD. The course of absorptance is very similar in all three systems, but the position of the global minima and local extrema shifts to smaller polar angles by increasing the periodicity. Namely, the narrow local maxima (37%, 34.7%, 34%) appear at 28.9°, 20.4° and 14.7° polar angles (V$_{600/660/710}$ points, according to the nomination in ref. 20), indicating that their appearance is governed by grating-coupling phenomenon. The local maxima override the absorptance attainable at perpendicular incidence in 660-nm and 710-nm-pitch designs, indicating that tilting is advantageous in these NCAI-SNSPDs. The position of the global absorptance maxima (68.4%, 67.7%, 67.6%) is only slightly influenced by the periodicity, all global maxima appear at similar polar angles (PBA$_{600/660/710}$ points: 77°, 78°, 79°) in the region of NbN-related ATIR phenomenon.
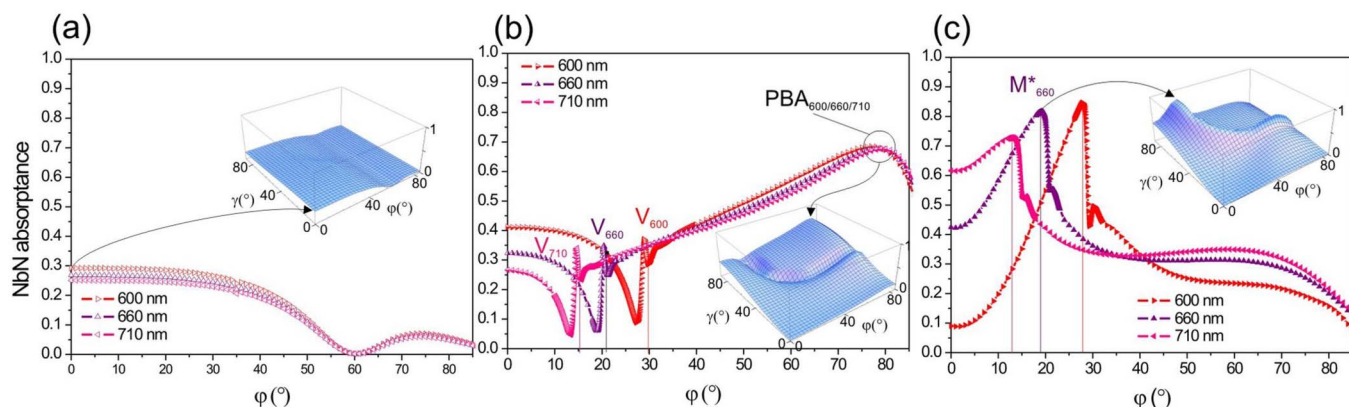
Figure 5 | NbN absorptance in three different long 3p-periodic SNSPD designs. (a) OC-SNSPD in P-orientation, (b) NCAI-SNSPD in S-orientation, and (c) NCDAI-SNSPD in S-orientation. The insets indicate the polar-azimuthal angle dependent NbN absorptance in 660-nm-pitch designs.

In long-periodic NCDAI-SNSPDs the NbN absorptance observable at perpendicular incidence is larger than in corresponding NCAI-SNSPDs, except in 600-nm-pitch design (Fig. 5c-to-5b, Supplementary Fig. S1a), and by increasing the polar angle increases further through large global maxima (84.5%, 81.6%, 72.7%), which approximate the absorptances in corresponding short-periodic designs (Fig. 5c-to-3c). These global NbN absorptance maxima shift backward by increasing the periodicity, namely they appear at 27.9°, 19.3°, 12.9° polar angles corresponding to cut-off points on absorptance curves of counterpart short-periodic NCDAI-SNSPDs. In addition to this, local NbN absorptance maxima of 49.4%, 55.3%, 52.8% are attained at 30.3°, 21.6°, 15.8° polar angles in 3p-periodic NCDAI-SNSPD designs. These maxima appear after local minima at

orientations (29.3°, 21.2°, 15.4°) similar to the $V_{600/660/710}$ points in NCAI-SNSPDs, indicating that the local extrema have analogous physical origin in the two integrated device design types (Fig. 5c-to-5b). The global NbN absorptance maxima decrease by increasing the periodicity also in long-periodic NCDAI-SNSPDs, while the highest local NbN absorptance maximum is attained in 660-nm-pitch design.

The fill-factor normalized NbN absorptance is commensurate in OC-SNSPDS and NCAI-SNSPDs, while it is ~3 times larger in NCDAI-SNSPDs (Fig. 6a). The normalized absorptance indicates a shallow local maximum at 660-nm-pitch already in OC-SNSPD. In contrast, the normalized absorptance computed at the local maxima ($V_{660/660/710}$ points) monotonously increases in NCAI-SNSPD
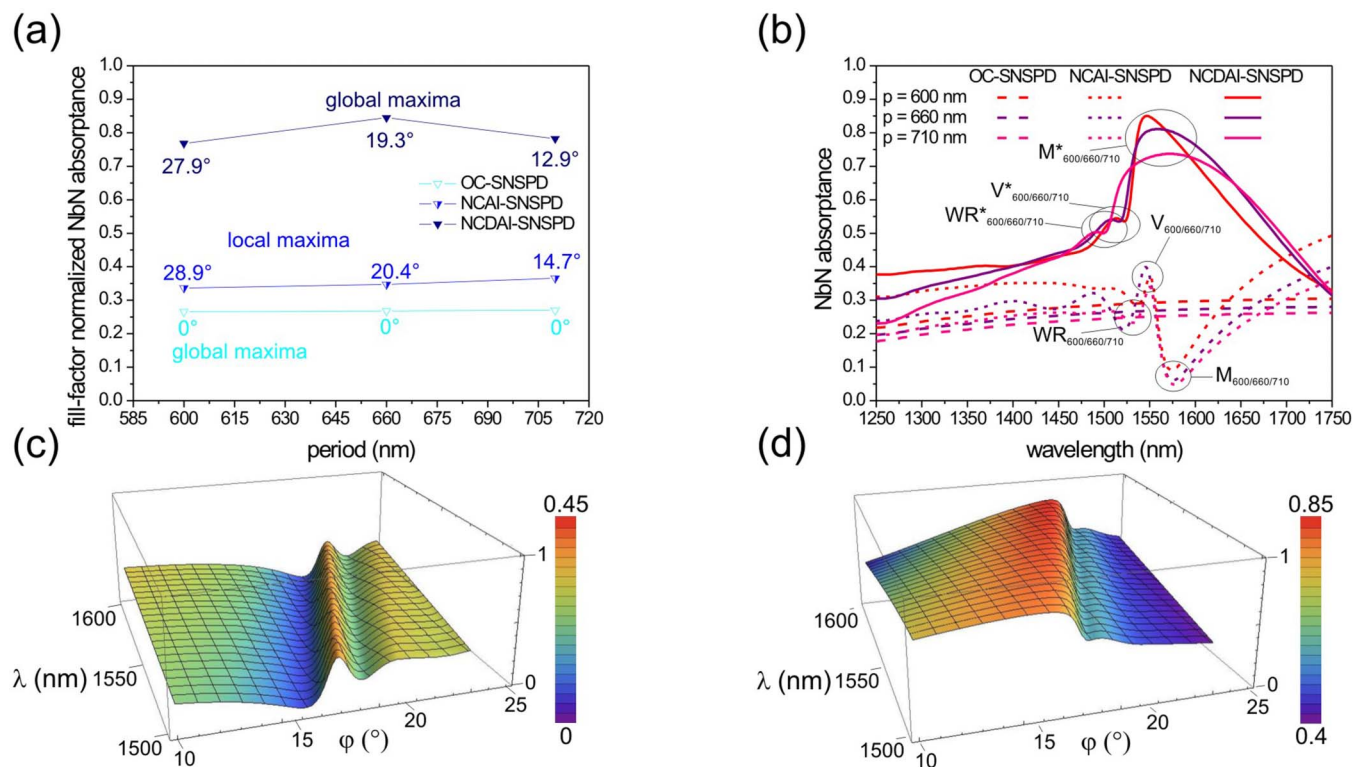

Figure 6 | (a) The NbN absorptance normalized by the fill-factor in 3p-periodic SNSPD designs. (b) Wavelength dependent absorptance at the orientations in different SNSPD designs indicated in (a). The absorptance as a function of φ polar angle and λ wavelength in 660-nm-pitch (c) NCAI-SNSPD and (d) NCDAI-SNSPD design.

designs. In *3p*-periodic NCDAI-SNSPDs, although the maximal absorptance decreases by increasing the periodicity, the fill-factor normalized NbN absorptance indicates a maximum, revealing to the particularity of 660-nm-pitch.

The spectral responses of OC-SNSPDs at perpendicular incidence indicate that the NbN absorptance monotonously increases with the wavelength, there are no significant changes at 1550 nm (Fig. 6b, dashed lines, Supplementary Fig. S1b). The spectral responses of NCAI-SNSPDs computed at the local maxima in polar angle indicate narrow local maxima ($V_{600/660/710}$ points), that appear within the error of computations at 1550 nm in all *3p*-periodic designs, separating shallow local ($WR_{600/660/710}$ points) and broad global minima ($M_{600/660/710}$ points) (Fig. 6b short dashed lines, Supplementary Fig. S1b, according to nominations in ref. 20).

The spectral responses of NCDAI-SNSPDs computed at the global NbN absorptance maxima in polar angle reach large global absorptance maxima ($M^*_{600/660/710}$ points: 1542 nm, 1556 nm, 1569 nm) in close proximity of the 1550 nm operation wavelength of SNSPD devices (Fig. 6b continuous lines, Supplementary Fig. S1b). Even though the maximum is slightly detuned from 1550 nm in 660-nm-pitch design as well, the large FWHM makes possible to attain the largest normalized absorptance at telecom wavelengths important in practical applications.

The device orientation dependence of the NbN absorptance spectra in 660-nm-pitch designs indicate that the polar angle corresponding to the local NbN absorptance maxima in NCAI-SNSPDs and to the large global maxima in NCDAI-SNSPDs increases linearly by increasing the wavelength (Fig. 6c, d).

Near-field phenomena in short-periodic designs. The near-field investigation has shown that there is an antinode on the normalized E-field at the bottom of quarter-photonic-wavelength nano-cavities in each short-periodic OC-SNSPDs (Fig. 7a/a–c).

The normalized E-field in short-periodic NCAI-SNSPDs indicates intense antinodes at the bottom of each quarter-plasmon-wavelength nano-cavity at the orientations corresponding to the global maxima (Fig. 7b/a–c). As the global maximum appears at 40° polar angle close to the condition of SPP excitation in 200-nm-pitch NCAI-SNSPD design, additional E-field enhancement, and forward propagating SPPs are observable above the horizontal gold segment (Fig. 7b/a, Video 1). There is no significant difference between the normalized E-field values in the three *p*-periodic NCAI-SNSPD designs (Fig. 7b/a–c). This is in accordance with the literature describing that the efficiency of collective resonances on sub-wavelength periodic MIM nano-cavity arrays only slightly depends on the periodicity in the investigated *p*-periodicity interval[14,22]. As a result of the collective resonances, there are no reflected waves below *p*-periodic NCAI-SNSPD designs (Video 1–3).

In NCDAI-SNSPD device designs the normalized E-field is further enhanced significantly in the nano-cavities neighboring the deflectors (Fig. 7c/a–c). The local field enhancements indicate that the gold deflectors not only perturb the E-field, they also absorb a part of the incoming light. This is in accordance with the smaller attainable NbN absorptance in short-periodic NCDAI-SNSPDs than without deflectors in NCAI-SNSPDs (Fig. 3c-to-b, 4b–d).

At the orientations corresponding to sudden NbN absorptance changes, surface waves with wave fronts perpendicular to the sapphire-interface are observable in all three *p*-periodic NCDAI-SNSPDs comprising *3p*-periodic deflectors, similarly to the counterpart long-periodic designs (see next section).

Intense backward propagating and weakly bounded waves appear in 200-nm-pitch design (Video 4), the surface waves indicate more bounded characteristics in 220-nm-pitch design (Video 5), while weak surface waves are superimposed with waves propagating towards the direction of specular reflection in 237-nm-pitch design (Video 6).
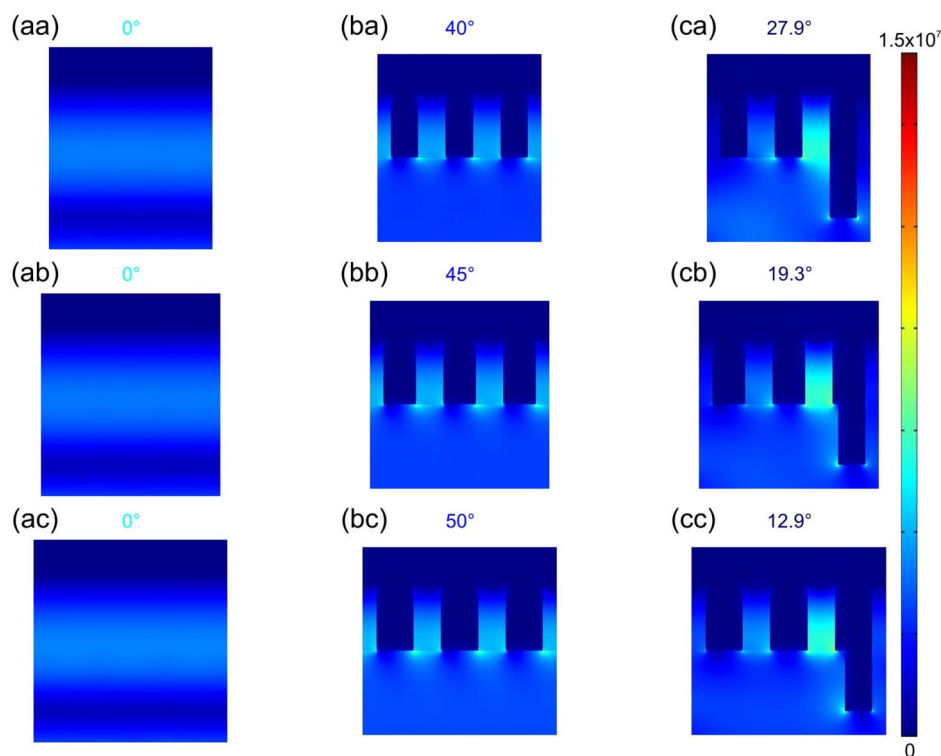

Figure 7 | Near-field distribution in short-periodic SNSPD designs at the NbN absorptance maxima in case of 1550 nm p-polarized illumination of (a/ a–c) OC-SNSPDs, (b/a–c) NCAI-SNSPDs (Video 1–3), (c/a–c) NCDAI-SNSPDs (Video 4–6); first row *p* = 200 nm, second row *p* = 220 nm, third row *p* = 237 nm.

Near-field phenomena in long-periodic designs. Intense antinodes are observable on the normalized E-field at the bottom of quarter-photonic-wavelength nano-cavities in each long-periodic OC-SNSPDs, similarly to their short-periodic counter-pairs (Fig. 8a/a–c, Supplementary Fig. S2d, Video7).

In long-periodic NCAI-SNSPDs, in addition to the enhanced normalized E-field at the bottom of each quarter-plasmon wavelength MIM nano-cavity, E-field enhancement is observable also below the NbN segments. This is due to the surface waves propagating backward with wave-fronts perpendicular to the sapphire interface at the orientations corresponding to the local absorptance maxima ($V_{600/660/710}$ points, Fig. 8b/a–c, Video 8–10, Supplementary Fig. S2f, Video 9).

In our previous work we have shown that in 600-nm-pitch design the narrow local maximum (V_{600} point) appears at tilting, where the integrated grating couples to surface waves having a wavelength slightly larger than the light wavelength in sapphire[50]. The metallic dielectric property is not required condition of their appearance indicating that these surface waves are analogous with Brewster-Zenneck modes (see Supplementary material)[52,53]. These results show that different surface waves constituting a composite diffractive field are capable of resulting in local near-field enhancement, in accordance with the literature[9].

In 3p-periodic NCDAI-SNSPDs the normalized E-field indicates enhancement at the bottom of each MIM nano-cavity. In addition to this, at the global NbN absorptance maxima in polar angle the time evolution of the E-field shows weakly bound backward propagating surface waves with wave-fronts perpendicular to the sapphire interface and having a wavelength equal to the SPP wavelength (Fig. 8c/a–c, Video 11–13, Supplementary Fig. S2i, Video 12).

These results indicate that in all three 3p-periodic NCDAI-SNSPDs the E-field is confined above the NbN segments due to the resonant oscillation of nano-plasmonic modes in the MIM nano-cavities, and below the NbN segments via composite diffracted field comprising propagating surface waves synchronized with them.

Discussion

In OC-SNSPDs the optimized quarter-photonic-wavelength of the gold reflector covered nano-cavity ensures that the E-field antinodes overlap with the NbN stripes (Fig. 7a, 8a, Supplementary Fig. S2d, Video 7), which makes possible to attain absorptance higher than in bare-SNSPDs[46,47]. At $\gamma = 0°$ azimuthal angle the parallelism of the E-field oscillation direction to the NbN stripes in P-orientation promotes the E-field penetration. Illumination with perpendicularly incident beams is optimal in all OC-SNSPDs (Fig. 2–8/a). The fill-factor normalized absorptance exhibits a local maximum at 660-nm-pitch (Fig. 6a), i.e. this design is advantageous for practical applications requiring minimized kinetic inductance in OC-SNSPDs.

In NCAI-SNSPDs and NCDAI-SNSPDs the resonance in MIM nano-cavities with optimized quarter-plasmonic-wavelength ensures that the high-intensity E-field antinodes are coincident with the NbN segments located at their entrance (Fig. 7b,c, 8b,c, Video 1–6, 8–13, Supplementary Fig. S2e–i, Video 9, 12, 14–16)[11,12,23,48–50]. To maximize the E-field enhancement originating from cavity resonant plasmonic modes, the E-field oscillation direction has to be perpendicular to the integrated gold segments, which explain that $\gamma = 90°$ azimuthal angle corresponding to S-orientation is advantageous in these designs. The coupled resonances on sub-wavelength periodic, quarter-plasmonic-wavelength MIM nano-cavities result in almost polar angle independent perfect absorptance in all p-pitch NCAI- and NCDAI-SNSPDs (Fig. 3b, c)[14,22], while the weak coupling in 3p-periodic NCAI- and NCDAI-SNSPDs causes stronger NbN absorptance dependence on tilting (Fig. 5b, c)[12,13,50].

The NbN absorptance modulation in 3p-periodic NCAI-SNSPD device structures is closely related to the classical Wood-anomalies on the integrated nano-cavity-grating[54–59]. As a result of cavity resonances occurring at 1550 nm wavelength, strong optical response modulation and opening of plasmonic band-gaps (PBG) is observable, since different surface waves are grating-coupled on the integrated 3p-periodic patterns, which interact with the localized plasmonic modes[9,20].
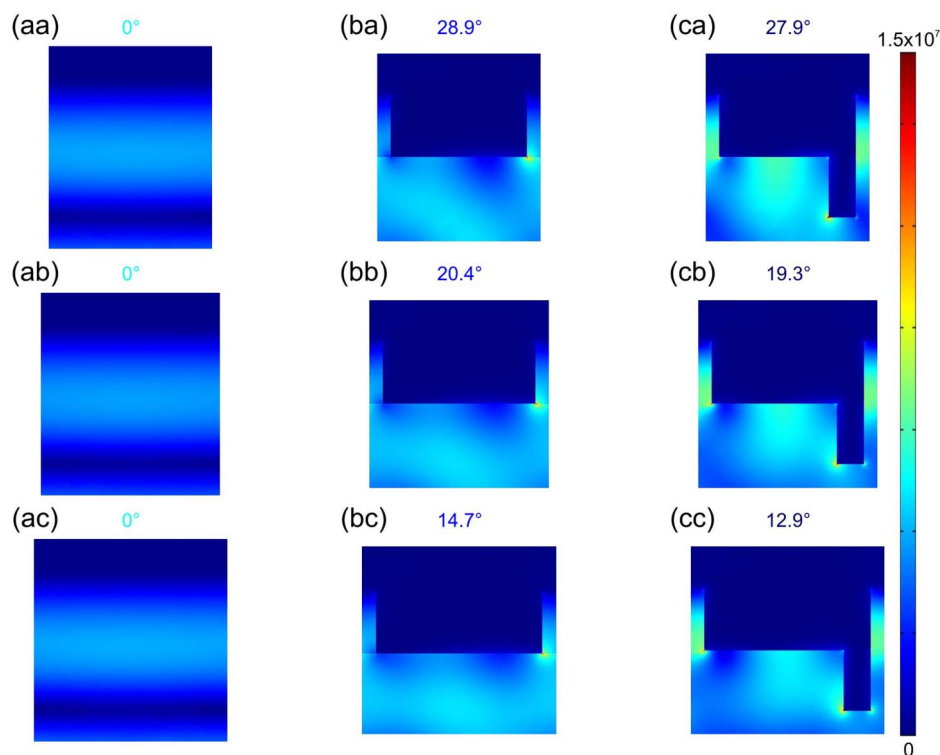

Figure 8 | Near-field distribution in case of 1550 nm p-polarized illumination of long-periodic SNSPD designs (a/a–c) perpendicular incidence onto OC-SNSPDs, **(b/a–c)** local maxima ($V_{600/660/710}$ points) in NCAI-SNSPDs (Video 8–10), **(c/a–c)** global maxima in NCDAI-SNSPDs (Video 11–13); first row $p = 600$ nm, second row $p = 660$ nm, third row $p = 710$ nm.

The Fano-like spectra computed at polar angles corresponding to $V_{600/660/710}$ points in long-periodic NCAI-SNSPDs indicate the superposition of resonant and nonresonant modes (Fig. 6b, Supplementary Fig. S1b)[55,57].

In all investigated $3p$-periodic NCAI-SNSPDs there are specific orientations, where series of nano-cavities are synchronously illuminated, making possible excitation of collective cavity resonances. These orientations can be computed as[50]:

$$\sin \varphi^{m,k} = \frac{m\frac{\lambda}{n_{sapphire}}}{k \cdot p}. \qquad (1)$$

The observed local NbN absorptance maxima ($V_{600/660/710}$ points) appearing in 600, 660, 710 nm-pitch-designs correspond to $m = 1$, $k = 3, 4, 5$ series.

The wavelength of surface waves that might be grating-coupled at the observed extrema can be calculated based on the momentum conservation criterion: $k_{surface\ wave} = k_{photon} \pm k_{grating}$. The time-evolution of the E-field indeed shows backward propagating surface waves at the substrate interface, however with different wavelength and intensity at different types of extrema (Video 8–10, Supplementary Fig. S2e–g, Video 9, 14, 15), which originate from -1 order grating-coupling on $3p$-periodic grating according to:

$$-\frac{2\pi}{\lambda_{surface\ wave}} = \frac{2\pi n_{sapphire}}{\lambda} \sin \varphi - \frac{2\pi}{3p}. \qquad (2)$$

Based on this relationship the waves coupled at the orientation corresponding to global minima in polar angle, coincident with the $M_{600/660/710}$ centers of PBGs, have a wavelength equal to that of SPPs at sapphire-gold interface (Fig. 5b and 6b, Supplementary Fig. S1). However, at the global minima the normalized E-field is confined below the gold segments, and propagating waves emanating towards the direction corresponding to specular reflection are observable in all three $3p$-periodic NCAI-systems (Supplementary Fig. S2e, Video 14). This is caused by the leaky nature of surface waves grating-coupled under these conditions, and shows that the confinement below gold causes re-radiation and prevents efficient light-coupling into the cavities[20,50]. These near-field observations are in accordance with the intrinsic phase difference between the SPPs and non-plasmonic surface waves in the composite diffracted field described in the literature[9,58,59]. However, SPPs are coupled dominantly through the periodicity of the grating only at specific orientations specified by Eq. 2, in accordance with the dynamical diffraction theory[56].

The weakly bounded surface waves at the local maxima ($V_{600/660/710}$ points) have wavelengths slightly larger than the photonic modes, showing that surface waves analogous with Brewster-Zenneck modes are dominantly coupled in the composite diffracted field (Fig. 8b, Supplementary Fig. S2f, g, Video 9, 15)[52,53]. These backward propagating surface waves are better synchronized with the nano-cavities, which makes larger local E-field enhancement possible around the NbN segments at the sharp PBG edges indicated by $V_{600/660/710}$ points.

The global NbN absorptance maxima appear in NCAI-SNSPDs at tilting corresponding to the plasmonic Brewster angle (BPA, Fig. 5c)[60]. The E-field time-evolution indicates forward propagating waves, that ensure E-field enhancement both inside and below the nano-cavities at PBA (Supplementary Fig. S2h, Video 16). The complementary spectral studies revealed that this phenomenon is observable in a very broad wavelength interval (Supplementary Fig. S1b), however single-photon detection at PBA is experimentally hardly implementable.

The cut-off points of NbN absorptance in p-periodic, and the global NbN absorptance maxima in $3p$-periodic NCDAI-SNSPDs appear at the orientations where surface waves with wavelength equal to SPP wavelength can be grating-coupled according to Eq. 2

(Fig. 3c and 5c, Supplementary Fig. S1a). In all NCDAI-SNSPD designs the deflectors result in enormous E-field enhancement below the NbN segments via composite surface waves (Fig. 7c, 8c, Video 4–6 and 11–13, Supplementary Fig. S2i, Video 12). This is due that in presence of deflectors the spatial synchronization of propagating plasmonic modes with respect to the MIM nano-cavities is ensured. Additionally, the SPPs are efficiently converted into non-plasmonic surface waves due to grazing incidence onto the deflectors (see Supplementary material). As a result, the deflectors maximize the effective NbN extinction cross-section via spatial synchronization between the localized modes and the backward propagating composite surface waves, and ensure enhanced power-flow into the MIM-cavities as well. The presented examples prove that compensation of losses caused by three-times smaller fill-factor might be realized.

In conclusion, the optimal cavity-lengths and illumination directions were determined for p-polarized light illumination of three types of SNSPDs designs, and an optimal periodicity was determined for $3p$-periodic OC- and NCDAI-SNSPDs.

We have shown that the E-field concentration around the NbN segments at the bottom of gold reflector covered ~quarter-photonic-wavelength nano-cavities results in the highest absorptance at perpendicular incidence onto OC-SNSPDs in P-orientation. Although the absorptance decreases by increasing the periodicity in OC-SNSPDs, the presented results indicate that 660-nm-pitch design is optimal in $3p$-periodicity interval.

Our present study has confirmed that in NCAI-SNSPDs the collective resonances' efficiency on MIM nano-cavity-arrays in S-orientation strongly depends on the periodicity. Almost polar angle independent perfect absorptance is attainable in p-periodicity interval, while the $3p$-periodic integrated patterns act as plasmonic band-gap structures, where perpendicular incidence already results in moderate absorptance enhancement, while coupling to surface waves is capable of resulting in local and global NbN absorptance enhancements at specific ($V_{600/660/710}$ and $PBA_{600/660/710}$) orientations. Our present results have shown that the narrow local maxima are due to EM-field enhancement originating from surface waves analogous with Brewster-Zenneck modes rather than from surface plasmon polaritons. The $3p$-periodic integrated patterns, which are optimal for plasmonic band-gap engineering, result in moderate normalized absorptance caused by radiative out-coupling of SPPs, which are spatially desynchronized with respect to the NbN pattern.

We have proven that the re-radiation of plasmons can be prevented by deflectors in NCDAI-SNSPDs. The gold deflectors act simultaneously as good plasmonic mirrors and mode converters, and ensure high intensity synchronous E-field below the absorbing NbN stripes via composite surface waves. The attainable absorptance strongly depends on the NbN patterns' periodicity in these designs. Namely, the deflector-related absorption loss overcomes the resulted enhancement in p-periodic NCDAI-SNSPDs, while huge absorptance enhancement is reached in $3p$-periodic NCDAI-SNSPDs via spatial synchronization. The peculiarity of 660-nm-pitch NCDAI-SNSPD design is that the cavity resonance condition is maintained laterally as well, due to the 1.5 λ_{SPP} distance between deflectors neighboring each of the nano-cavities[59].

Our results prove that the PBG features can be completely inverted, and the absorptance minima related to the PBG center in NCAI-SNSPDs can be converted into maxima via properly designed integrated nano-cavity-deflector-array in NCDAI-SNSPDs. The developed method is a general principle, which might be applied to eliminate radiation losses from nano-photonical systems based on plasmonic structures.

Methods

The FEM modeling was performed by applying the Radiofrequency module of Comsol Multiphysics software package (Comsol AB). The optimal illumination direction of each design was determined using a parametric sweep in three-dimensional

computations, namely by tuning the φ polar and γ azimuthal angles during p-polarized 1550 nm wavelength light illumination of the SNSPD devices in conical mounting (Fig. 1, 2g, h). First the optimal azimuthal orientation was selected by calculations performed over the $\gamma = [0^\circ - 90^\circ]$ and $\varphi = [0^\circ - 85^\circ]$ intervals, with $\Delta\gamma = \Delta\varphi = 5^\circ$ resolution (Fig. 3 and 5 insets). Then the optimal tilting was determined by varying the polar angle in $\varphi = [0^\circ, 85^\circ]$ region with 1° resolution.

Finally higher (0.05°) resolution FEM calculations were performed in intervals surrounding the local/global NbN absorptance maxima in order to inspect the accompanying near-field phenomena in details (Fig. 3 and 5, Supplementary Fig. S1a).

Wavelength dependent FEM computations were also performed at specific orientations of each designs corresponding to NbN absorptance extrema predicted by angle dependent studies (Fig. 4b–d and 6b–d, Supplementary Fig. S1b). These calculations were performed with 5 nm resolution in the $\lambda = [1250-1750 \text{ nm}]$ region.

The wavelength dependent optical parameters were taken into account by integrating Cauchy formulae for dielectrics (HSQ and sapphire), and loading tabulated data-sets for metals (NbN and gold) into the models. Detailed spectral study was performed by tuning the wavelength and angle of incidence simultaneously in narrow [$15^\circ \times 100$ nm] intervals surrounding the conditions of significant NbN absorptance modifications in NCAI- and NCDAI-SNSPDS (Fig 4c, d, Fig. 6c, d).

In present numerical model computations NbN segments with 4 nm thickness and 100 nm width comprising a $\sim$2 nm thick NbNO$_x$ cover-layer were taken into account (Fig. 1 and 2i). The period of the NbN pattern was also varied for each SNSPD-design type, the three different periodicities inspected in details were 200 nm, 220 nm, 237 nm in case of p, and 600 nm, 660 nm, 710 nm in case of $3p$ periodic patterns. The width of the individual NbN stripes was kept constant, as a consequence by increasing the periodicity the fill-factor was decreasing.

In OC-SNSPDs previously optimized nano-cavity geometry was applied, namely the single continuous nano-cavity filled with hydrogen-silsesquioxane (HSQ) was $\sim$279 nm long i.e. $\sim$quarter-photonic-wavelength, and was closed by a 60 nm thick gold reflector (Fig. 2a, d). The 200-nm-pitch OC-SNSPD was also experimentally studied in our previous work[45].

In NCAI-SNSPDs the NbN stripes are aligned at the bottom of MIM nano-cavities with optimized length, namely each nano-cavity filled with HSQ was $\sim$220 nm long i.e. $\sim$quarter-plasmon-wavelength, and was closed by 226 nm long vertical and 60 nm thick horizontal gold segments. The alternating HSQ and intersecting gold segments compose a plasmonic MIM nano-cavity-array with p and $3p$-periodicity (Fig. 1 and 2b, e). The 200 nm and 600 nm NCAI-SNSPDs were introduced in refs. 48–50, the 600-nm-pitch NCAI-SNSPD was also experimentally studied in our previous work[49]. Detailed comparative study of the absorptances in 200-nm, 220-nm and 237-nm-pitch designs, as well as in 600-nm, 660-nm and 710-nm-pitch NCAI-SNSPDs is performed in present work.

In NCDAI-SNSPDs the NbN stripes are aligned at the bottom of MIM nano-cavities with optimized length, while the periodicity was shown to be optimal in case of 660-nm-pitch design to attain the largest normalized absorptance. Novel approach is the integration of 220 nm long and 100 nm wide deflector segments with $3p$-periodicity into both p and $3p$ periodic NbN patterns, i.e. reinserting the gold segment missing from the cavities into the substrate region (Fig. 1 and 2c, f). Experimental studies on $3p$-periodic NCAI- and NCDAI-SNSPD design types are in progress. The alignment accuracy attainable via e.g. Raith lithography tools in two-step e-beam lithography procedure is on the order of, or moreover better than $\sim$100 nm, which makes possible appropriate overlay of the $3p$ periodic deflector-array with the long-periodic pattern of NCAI-SNSPDs.

The normalization according to the fill-factor is performed by computing the (NbN absorptance in specific design)*[Fill-factor$_{NbN}$(660 nm)/Fill-factor$_{NbN}$(specific design)] quantity, namely by approximating the efficiency for the case of analogous pattern with 660 nm periodicity.

To perform time-averaged near-field study the normalized E-field was extracted via standard post-processing tool of COMSOL software package, while for near-field time-evolution inspection the $\sqrt{E_x^2 + E_y^2 + E_z^2}$ quantity was manually extracted with 5° phase-resolution.

The inspected plasmon enhanced absorption phenomena originate from the integrated noble metal elements, namely from the reflector, grating and deflector. However, it is possible to apply versatile substrate materials (e.g. silica) and various superconducting absorbing segments (e.g. WSi[43]), which make high precision fabrication via e-beam lithography realizable. To ensure the right angle of incidence during illumination, coupling via obliquely cut optical fibers are the most appropriate (Fig. 1).

1. Ebbesen, T. W., Lezec, H. J., Ghaemi, H. F., Thio, T. & Wolff, P. A. Extraordinary optical transmission through sub-wavelength hole arrays. *Nature* **391**, 667–669 (1998).
2. Barnes, W. L., Dereux, A. & Ebbesen, T. W. Surface plasmon subwavelength optics. *Nature* **424**, 824–830 (2003).
3. Ozbay, E. Plasmonics: Merging photonics and electronics at nanoscale dimensions. *Science* **311**, 189–193 (2006).
4. Maier, S. A. Plasmonics: Fundamentals and applications (Springer, New York, 2007).
5. Polman, A. Applied Physics: Plasmonics applied. *Science* **322**, 868–869 (2008).
6. Garcia-Vidal, F. J., Martin-Moreno, L., Ebbesen, T. W. & Kuipers, L. Light passing through subwavelength apertures. *Reviews of Modern Physics* **82**, 729–787 (2010).
7. Bravo-Abad, J., Martin-Moreno, L. & Garcia-Vidal, F. J. Transmission properties of a single metallic slit: From the subwavelength regime to the geometrical-optics limit. *Phys. Rev E* **69**, 026601 (2004).
8. Gordon, R. Light in subwavelength slit in metal: propagation and reflection. *Phys. Rev. B* **73**, 153405 (2006).
9. Gay, G. *et al.* The optical response of nanostructures surfaces and the composite diffracted evanescent wave model. *Nat. Phys.* **2**, 262–267 (2006).
10. White, J. S. Extraordinary optical absorption through sub-wavelength slits. *Opt. Lett.* **34**, 686–688 (2009).
11. Kurokawa, Y. & Miyazaki, H. T. Metal-insulator-metal plasmon nanocavities: Analysis of optical properties. *Phys. Rev. B* **75**, 035411 (2007).
12. Miyazaki, H. T. & Kurokawa, Y. Controlled plasmon resonance in closed metal/insulator/metal nanocavities. *Appl. Phys. Lett.* **89**, 211216 (2006).
13. Schroter, U. & Heitmann, D. Surface-plasmon-enhanced transmission through metallic gratings. *Phys. Rev. B* **58**, 15419–15421 (1998).
14. Porto, J. A., Garcia-Vidal, F. J. & Pendry, J. B. Transmission resonances on metallic gratings with very narrow slits. *Phys. Rev. Lett.* **83**, 2845–2848 (1999).
15. Collin, S., Pardo, F., Teissier, R. & Pelouard, J. L. Strong discontinuities in the complex photonic band structure of transmission metallic gratings. *Phys. Rev. B* **63**, 033107 (2001).
16. Collin, S., Pardo, F. & Pelouard, J. L. Resonant-cavity-enhanced subwavelength metal–semiconductor–metal photodetector. *Appl. Phys. Lett.* **83**, 1521–3 (2003).
17. Marquier, F., Greffet, J.-J., Collin, S., Pardo, F. & Pelouard, J. L. Resonant transmission through a metallic film due to coupled modes. *Opt. Express* **13**, 70–76 (2005).
18. Pang, Y., Genet, C. & Ebbesen, T. W. Optical transmission through subwavelength slit apertures in metallic films. *Opt. Commun.* **280**, 10–15 (2007).
19. Fernández-Domínguez, A. I., Garcia-Vidal, F. J. & Martín-Moreno, L. Resonant transmission of light through finite arrays of slits. *Phys. Rev. B* **76**, 235430 (2007).
20. de Ceglia, D., Vincenti, M. A., Scalora, M., Akozbek, N. & Bloemer, M. J. Plasmonic band edge effects on the transmission properties of metal gratings. *AIP Advances* **1**, 032151 (2011).
21. Tan, W.-C., Preist, T. W., Sambles, J. R. & Wanstall, N. P. Flat surface-plasmon-polariton bands and resonant optical absorption on short-pitch metal gratings. *Phys. Rev. B* **59**, 12661 (1999).
22. Garcia-Vidal, F. J. & Martín-Moreno, L. Transmission and focusing of light in one-dimensional periodically nanostructured metals. *Phys. Rev. B* **66**, 155412 (2002).
23. Hibbins, A. P. *et al.* Resonant absorption of electromagnetic fields by surface plasmons buried in a multilayered plasmonic structure. *Phys. Rev. B* **74** (2006).
24. Popov, E., Bonod, N. & Enoch, S. Comparison of plasmon surface waves on shallow and deep metallic 1D and 2D gratings. *Opt. Exp.* **15**, 4224–4237 (2007).
25. Genevet, P. *et al.* Large enhancement of nonlinear optical phenomena by plasmonic nanocavity gratings. *Nano Letters* **10**, 4880–4883 (2010).
26. DiMaio, J. R. & Ballato, J. Polarization-dependent transmission through subwavelength anisotropic aperture arrays. *Opt. Express* **14**, 2380 (2006).
27. Matterson, B. J. *et al.* Increased Efficiency and Controlled Light Output from a Microstructured Light-Emitting Diode. *Adv. Mater* **13/2**, 123–127 (2001).
28. Hsu, S.-Y., Lee, M.-C., Lee, K.-L. & Wei, P.-K. Extraction enhancement in organic light emitting devices by using metallic nanowire arrays. *Appl. Phys. Lett.* **92**, 013303 (2008).
29. Yu, N. *et al.* Bowtie plasmonic quantum cascade laser antenna. *Optics Express* **15/20**, 13272–13281 (2007).
30. Chang, D. E., Sorensen, A. S., Hemmer, P. R. & Lukin, M. D. Quantum Optics with Surface Plasmons. *Phys. Rev. Lett.* **97**, 053002 (2006).
31. Colas de Francs, D. *et al.* Optical gain, spontaneous and stimulated emission of surface plasmon polaritons in confined plasmonic waveguide. *Optics Express* **18/16**, 16327–116334 (2010).
32. Yu, N. *et al.* Small-divergence semiconductor lasers by plasmonic collimation. *Nat. Photonics* **2**, 564–570 (2008).
33. Lal, S., Link, S. & Halas, N. J. Nano-optics from sensing to waveguiding. *Nature Photon.* **1**, 641–648 (2007).
34. Stuart, H. R. & Hall, D. G. Island size effects in nanoparticle-enhanced photodetectors. *Appl. Phys. Lett.* **73**, 3815–3817 (1998).
35. Ishi, T., Fujikata, J., Marita, K., Baba, T. & Ohashi, K. Si nano-photodiode with a surface plasmon antenna. *Jpn. J. Appl. Phys.* **44**, L364–L366 (2005).
36. Tang, L. *et al.* Nanometre-scale germanium photodetector enhanced by a near-infrared dipole antenna. *Nature Photon.* **2**, 226–229 (2008).
37. Yu, Z., Veronis, G., Fan, S. & Brongersma, M. L. Design of midinfrared photodetectors enhanced by surface plasmons on grating structures. *Appl. Phys. Lett.* **89**, 151116 (2006).
38. Bhat, R. D. R., Panoiu, N. C., Brueck, S. R. J. & Osgood, R. M. Jr. Enhancing the signal-to-noise ratio of an infrared photodetector with a circular metal grating. *Optics Express* **16**, 4588–4596 (2008).
39. Laux, E., Genet, C., Skauli, T. & Ebbesen, T. W. Plasmonic photon sorters for spectral and polarimetric imaging. *Nature Photonics* **2**, 161–164 (2008).
40. Konstantatos, G. & Sargent, E. H. Nanostructured materials for photon detection. *Nature Nanotechnology* **5**, 391–400 (2010).
41. Gol'tsman, G. N. *et al.* Picosecond superconducting single-photon optical detector. *Appl. Phys. Lett.* **79**, 705–708 (2001).

42. Pernice, W. H. P. *et al.* High-speed and high-efficiency travelling wave single-photon detectors embedded in nanophotonic circuits. *Nature Communications*, DOI:10.1038/ncomms2307.

43. Marsili, F. *et al.* Detecting single infrared photons with 93% system efficiency. *Nature Photonics*, DOI:10.1038/NPHOTO-2013-13.

44. Heeres, R. W. *et al.* On-Chip Single Plasmon Detection. *Nano Lett* **10**, 661–664 (2010).

45. Rosfjord, K. M. *et al.* Nanowire single-photon detector with an integrated optical cavity and anti-reflection coating. *Optics Express* **14**(2), 527–534 (2006).

46. Csete, M., Sipos, Á., Najafi, F., Hu, X. & Berggren, K. K. Numerical method to optimize the polar-azimuthal orientation of infrared superconducting-nanowire single-photon detectors. *Appl. Opt.* **50**(29), 5949–5956 (2011).

47. Csete, M., Sipos, Á., Najafi, F. & Berggren, K. K. Optimized polar-azimuthal orientations for polarized light illumination of different Superconducting Nanowire Single-Photon Detector designs. *Journal of Nanophotonics* **6**/1, 063523 (2012).

48. Hu, X., Holzwarth, C. W., Masciarelli, D., Dauler, E. A. & Berggren, K. K. Efficiently coupling light to superconducting nanowire single-photon detectors. *IEEE Trans. Appl. Supercond.* **19**(3), 336–340 (2009).

49. Hu, X., Dauler, E. A., Molnar, R. J. & Berggren, K. K. Superconducting nanowire single-photon detectors integrated with optical nano-antennas. *Optics Express* **19**(1), 17–31 (2011).

50. Csete, M., Sipos, Á., Szalai, A. & Szabó, G. Impact of polar-azimuthal illumination angles on efficiency of nano-cavity-array integrated single-photon detectors. *Optics Express* **20**/15, 17065–17081 (2012).

51. Driessen, E. F. C. & de Dood, M. J. A. The perfect absorber. *Appl. Phys. Lett.* **94**, 171109 2009).

52. Welford, K. R. Surface Plasmon-Polaritons. *IOP Short Meeting Series* **9**, 25–78 (1988).

53. Sarrazin, M. & Vigneron, J.-P. Light transmission by Brewster-Zenneck modes in chromium fiilms carrying a subwavelength hole-array. *Phys. Rev.* **71**, 075404 (2005).

54. Wood, R. W. Anomalous diffraction gratings. *Phys. Rev.* **15**, 928–937 (1935).

55. Fano, U. The theory of anomalous diffraction gratings and of quasi-stationary waves on metallic surfaces (Sommerfeld's waves). *J. Opt. Soc. Am.* **31**, 213–222 (1941).

56. Treacy, M. M. Dynamical diffraction explanation of the anomalous transmission of light through metallic gratings. *Phys. Rev. B* **66**, 195105 (2002).

57. Sarrazin, M., Vigneron, J.-P. & Vigoureux, J.-M. Role of Wood anomalies in optical properties of thin metallic films with a bidimensional array of subwavelength holes. *Phys. Rev. B* **67**, 085415 (2003).

58. Darmayan, S. A., Neviére, M. & Zayats, A. V. Analytical theory of optical transmission through periodically structured metal films via tunnel coupled surface plasmon modes. *Phys. Rev. B* **70**, 075103 (2004).

59. Pacifici, D., Lezec, H. J., Atwater, H. A. & Weiner, J. Quantitative determination of optical transmission through subwavelength slit arrays in Ag film: The essential role of surface wave interference and local coupling between adjacent slits. *Phys. Rev. B* **77**, 115411 (2008).

60. Alú, A., Aguanno, G. D., Mattiucci, N. & Bloemer, M. Plasmonic Brewster angle: Broadband extraordinary transmission through optical gratings. *Phys. Rev. Lett.* **106**, 123902 (2011).

Acknowledgements

Author contributions

Additional information

How to cite this article: Csete, M. *et al.* Improvement of infrared single-photon detectors absorptance by integrated plasmonic structures. *Sci. Rep.* **3**, 2406; DOI:10.1038/srep02406 (2013).